

Radio Emission from the First Quasars at $z = 6 - 15$

Muhammad A. Latif,¹* Daniel J. Whalen,² Mar Mezcua^{3,4}

¹Physics Department, College of Science, United Arab Emirates University (UAEU), PO Box 15551, Al-Ain, UAE

²Institute of Cosmology and Gravitation, University of Portsmouth, Dennis Sciama Building, Portsmouth PO1 3FX, UK

³Institute of Space Sciences (ICE, CSIC), Campus UAB, Carrer de Magrans, 08193 Barcelona, Spain

⁴Institut d'Estudis Espacials de Catalunya (IEEC), Carrer Gran Capità, 08034 Barcelona, Spain

Accepted XXX. Received YYY; in original form ZZZ

ABSTRACT

Nearly 300 quasars have now been found at $z > 6$, including nine at $z > 7$. They are thought to form from the collapse of supermassive primordial stars to $10^4 - 10^5 M_{\odot}$ black holes at $z \sim 20 - 25$, which then rapidly grow in the low-shear environments of rare, massive halos fed by strong accretion flows. Sensitive new radio telescopes such as the Next-Generation Very Large Array (ngVLA) and the Square Kilometer Array (SKA) could probe the evolution of these objects at much earlier times. Here, we estimate radio flux from the first quasars at $z \sim 6 - 15$ at 0.5 - 12.5 GHz. We find that SKA and ngVLA could detect a quasar like ULAS J1120+0641, a $1.35 \times 10^9 M_{\odot}$ black hole at $z = 7.1$, at much earlier stages of evolution, $z \sim 14 - 16$, with 100 hr integration times in targeted searches. The advent of these new observatories, together with the *James Webb Space Telescope* (*JWST*), *Euclid*, and the *Roman Space Telescope* (*RST*), will inaugurate the era of $z \lesssim 15$ quasar astronomy in the coming decade.

Key words:

quasars: general — black hole physics — early Universe — dark ages, reionization, first stars — galaxies: formation — galaxies: high-redshift

1 INTRODUCTION

Nearly 300 quasars have now been discovered at $z > 6$, including nine at $z > 7$ (e.g., Yang et al. 2020; Wang et al. 2021 – see Fan et al. 2022 for a recent review). The seeds of these quasars are thought to be direct-collapse black holes (DCBHs) from the collapse of $10^4 - 10^5 M_{\odot}$ primordial stars (Whalen & Fryer 2012; Hosokawa et al. 2013; Woods et al. 2021; Herrington et al. 2023). But to reach $10^9 M_{\odot}$ by $z \sim 6 - 7$ they must also be located in rare, massive haloes at the nexus of strong accretion flows in low-shear environments (Tenneti et al. 2018; Lupi et al. 2021; Valentini et al. 2021; Latif et al. 2022a). A number of studies have shown that DCBHs could be found at $z \gtrsim 20$ in the near infrared (NIR) by *JWST* (Pacucci et al. 2015; Whalen et al. 2020b) and $z \lesssim 15$ by *Euclid*, and the *RST* (Vikaeus et al. 2022).

Radio-loud quasars (i.e., with radio fluxes 10 times greater than their optical blue-band emission – Gloude-mans et al. 2022; Bañados et al. 2023) have now also been found at $z > 6$, such as J0309+2717 ($z = 6.10$; Belladitta et al. 2020), J1427+3312 ($z = 6.12$; McGreer et al. 2006), J1429+5447 ($z = 6.18$; Willott et al. 2010), P172+18 ($z = 6.82$; Bañados et al. 2021), and VIK J2318+3113 ($z = 6.444$; Zhang et al. 2022). They typically have BH masses $\gtrsim 10^8 M_{\odot}$ and grow at nearly the Eddington rate (e.g., Bañados et al. 2021). Except for J0309+2717 (classified as a blazar; Spingola et al. 2020), the radio emission from these sources is dominated by compact cores and/or

small-scale jets (< 1 kpc). Although DCBH detections by SKA and ngVLA will be limited to $z \lesssim 8$, (Whalen et al. 2020a, 2021), these observatories in principle could detect more massive quasars at well above this redshift, at much earlier stages of their evolution. Here, we estimate radio flux from a $z \sim 7$ quasar like ULAS J1120+0641 (Mortlock et al. 2011) at earlier stages of growth, up to $z \sim 15$. Our calculations are timely, given the recent discovery of a lensed $4 \times 10^7 M_{\odot}$ BH candidate in UHZ1 at $z = 10.3$ (Bogdan et al. 2023). In Section 2 we discuss how we calculate radio emission from the BH and star-forming regions in its host galaxy. We present radio fluxes for a number of SKA and ngVLA bands as a function of redshift in Section 3 and then conclude in Section 4.

2 NUMERICAL METHOD

We estimate quasar radio fluxes from fundamental planes (FPs) of BH accretion with bolometric luminosities taken from Smidt et al. (2018), who were the first to reproduce the properties of a $z \sim 7$ quasar in a cosmological simulation (left panel of Figure 1). We use second-year *Planck* cosmological parameters: $\Omega_M = 0.308$, $\Omega_{\Lambda} = 0.691$, $\Omega_b h^2 = 0.0223$, $\sigma_8 = 0.816$, $h = 0.677$ and $n = 0.968$ (Planck Collaboration et al. 2016).

* E-mail: latifne@gmail.com

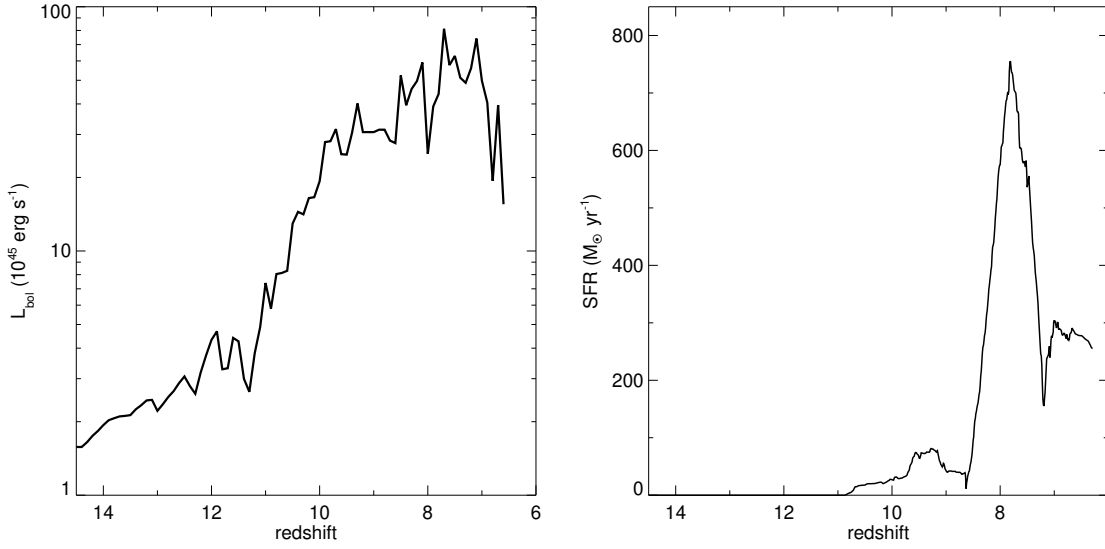


Figure 1. Bolometric luminosities, L_{bol} , for the quasar (left) and star formation rates in its host galaxy (right) as functions of redshift from [Smidt et al. \(2018\)](#).

2.1 BH Radio Flux

FPs of BH accretion are empirical relationships between the mass of a BH, M_{BH} , its nuclear X-ray luminosity at 2 - 10 keV, L_X , and its nuclear radio luminosity at 5 GHz, L_R ([Merloni et al. 2003](#); see [Mezcua et al. 2018](#) for a brief review). They cover six orders of magnitude in BH mass, including down to intermediate-mass black holes ($< 10^5 M_{\odot}$; [Gültekin et al. 2014](#)). To estimate the flux from the BH in a radio band in the Earth frame we first use the FP to calculate L_R in the source frame, which depends on M_{BH} and L_X . We obtain L_X from L_{bol} with Equation 21 of [Marconi et al. \(2004\)](#),

$$\log\left(\frac{L_{\text{bol}}}{L_X}\right) = 1.54 + 0.24\mathcal{L} + 0.012\mathcal{L}^2 - 0.0015\mathcal{L}^3, \quad (1)$$

where L_{bol} is in units of solar luminosity and $\mathcal{L} = \log L_{\text{bol}} - 12$. L_R can then be calculated from L_X with an FP of the form

$$\log L_R (\text{erg s}^{-1}) = \alpha \log L_X (\text{erg s}^{-1}) + \beta \log M_{\text{BH}} (M_{\odot}) + \gamma, \quad (2)$$

where α , β and γ for FPs from [Merloni et al. \(2003, MER03\)](#), [Körding et al. \(2006, KOR06\)](#), [Gültekin et al. \(2009, GUL09\)](#), [Plotkin et al. \(2012, PLT12\)](#), and [Bonchi et al. \(2013, BON13\)](#) are listed in Table 1 of [Whalen et al. \(2021\)](#). We also include the FP of Equation 19 in [Gültekin et al. \(2019, GUL19\)](#),

$$R = -0.62 + 0.70 X + 0.74 \mu, \quad (3)$$

where $R = \log(L_R/10^{38} \text{erg/s})$, $X = \log(L_X/10^{40} \text{erg/s})$ and $\mu = \log(M_{\text{BH}}/10^8 M_{\odot})$.

Since radio flux from a supermassive black hole (SMBH) that is cosmologically redshifted into a given observer band today does not originate from 5 GHz in the source frame at high redshifts, we calculate it from $L_R = \nu L_{\nu}$, assuming that the spectral luminosity $L_{\nu} \propto \nu^{-\alpha}$. Here, we consider $\alpha = 0.7$ ([Condon et al. 2002](#)) and $\alpha = 0.3$ ([Gloudemans et al. 2021](#)) for a reasonable range of spectral types. The spectral flux at ν in the observer frame is then calculated from the spectral luminosity at ν' in the rest frame from

$$F_{\nu} = \frac{L_{\nu'}(1+z)}{4\pi d_L^2}, \quad (4)$$

where $\nu' = (1+z)\nu$ and d_L is the luminosity distance.

2.2 H II Region Radio Emission

Thermal bremsstrahlung emission in H II regions can produce continuum flux whose spectral radio density can be derived from the ionizing photon emission rate in the H II region, Q_{Lyc} , from

$$L_{\nu} \lesssim \left(\frac{Q_{\text{Lyc}}}{6.3 \times 10^{52} \text{s}^{-1}}\right) \left(\frac{T_e}{10^4 \text{K}}\right)^{0.45} \left(\frac{\nu}{\text{GHz}}\right)^{-0.1} \quad (5)$$

in units of 10^{20}W Hz^{-1} ([Condon 1992](#)), where $Q_{\text{Lyc}} = \text{SFR} (M_{\odot} \text{yr}^{-1}) / 1.0 \times 10^{-53}$ ([Kennicutt 1998](#)) and SFR is the star formation rate. We estimate the radio continuum from star-forming regions in the host galaxy of the SMBH with the SFRs from [Smidt et al. \(2018\)](#) shown in the right panel of Figure 1, taking $T_e = 10^4 \text{K}$.

2.3 Supernova Radio Flux

Radio flux from early quasars could include synchrotron emission from young supernova (SN) remnants in the host galaxy. However, since SFRs in the galaxy are quite low until $z \sim 10 - 11$, we would not expect SNe to contribute much to the flux prior to these redshifts. [Condon \(1992\)](#) estimate the non-thermal radio luminosity from SNe in normal star-forming galaxies today to be

$$\left(\frac{L_N}{\text{W Hz}^{-1}}\right) \sim 4.4 \times 10^{34} \left(\frac{\nu}{\text{GHz}}\right)^{-\beta} \left[\frac{\text{SFR}(M > 5 M_{\odot})}{M_{\odot} \text{yr}^{-1}}\right], \quad (6)$$

where $\beta \sim 0.8$ is the spectral index. But Equation 6 would not be valid in the halo at early times because Pop III core-collapse SNe ([Joggerst et al. 2010](#); [Latif et al. 2022b](#)) only produced nJy radio fluxes ([Meiksin & Whalen 2013](#)) in the diffuse H II regions of high redshifts ([Whalen et al. 2004, 2008](#)), well below the detection limit of any planned survey. However, they may later approach those of Equation 6 at lower redshifts and near-solar metallicities so we adopt it for simplicity. Since the IMF of the stars in the host galaxy is unknown, we simply assume that they are above $5 M_{\odot}$ at all redshifts, so this constitutes a severe upper limit to the true SN flux.

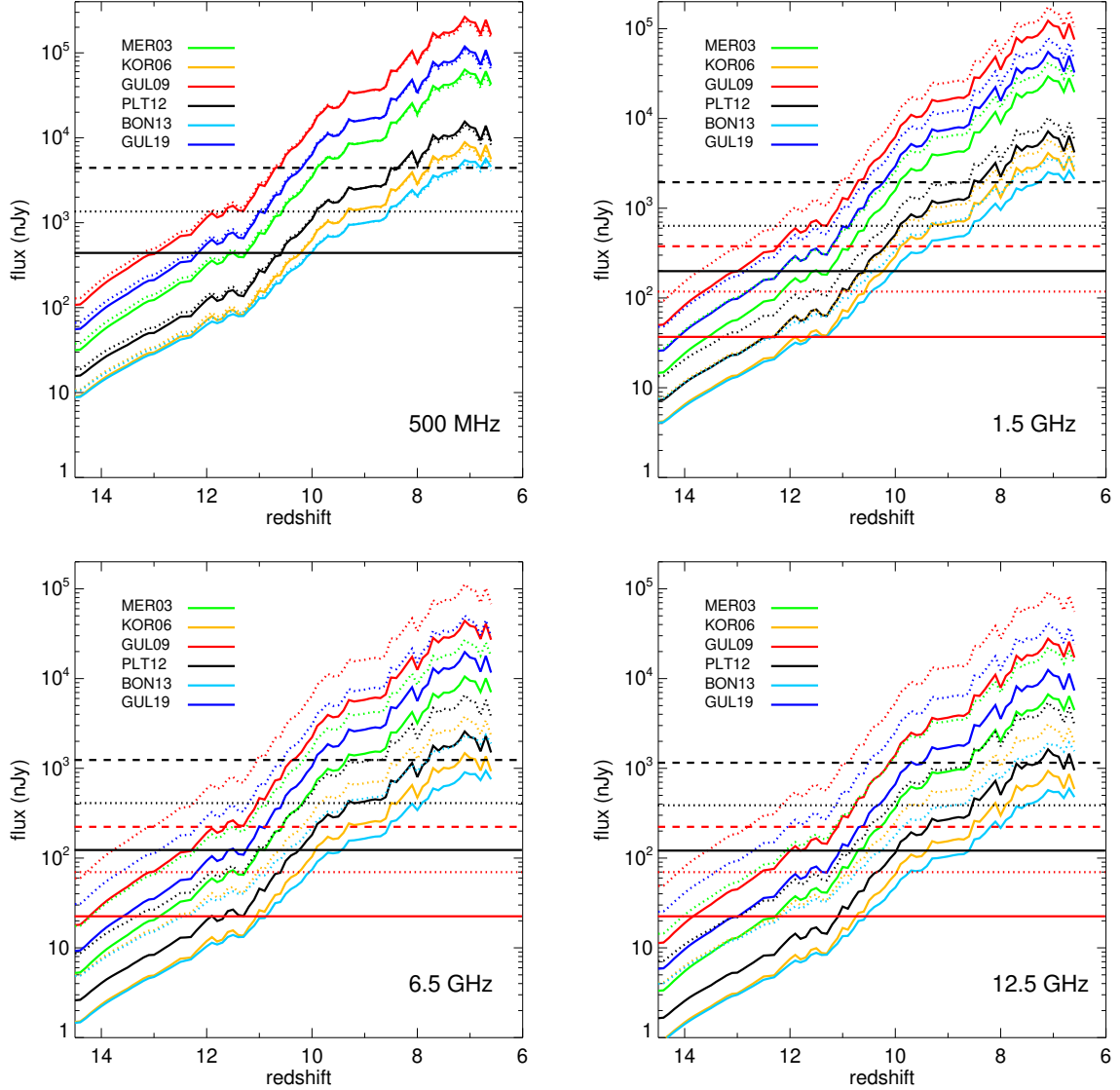


Figure 2. BH radio fluxes for $\alpha = 0.7$ (solid) and $\alpha = 0.3$ (dotted) from $z = 6 - 14.5$ at 500 MHz, 1.5 GHz, 2.5 GHz and 6.5 GHz. The dashed, dotted and solid horizontal lines are the detection limits for 1 hr, 10 hr and 100 hr integration times for SKA (black) and ngVLA (red) listed in Table 1.

3 RESULTS

We show F_ν at 500 MHz, 1.5 GHz, 6.5 GHz and 12.5 GHz at $z = 6 - 14.5$ for all six FPs and both choices of spectral index in Figure 2 along with the sensitivity limits for 1 hr, 10 hr, and 100 hr pointings by SKA and ngVLA listed in Table 1. For comparison, the most sensitive surveys by the Low-Frequency Array (LOFAR) will reach a few μJy below 1 GHz. The BH fluxes are higher at lower frequencies, where the estimates range from $\sim 9 - 120$ nJy at $z = 14.5$ to ~ 5 $\mu\text{Jy} - 0.2$ mJy at $z = 6$ at 500 MHz. At 6.5 GHz the fluxes are lower, $\sim 1.5 - 60$ nJy at $z = 14.5$ to ~ 0.8 $\mu\text{Jy} - 70$ μJy at $z = 6$. The choice of spectral index does not have much impact on the flux at 500 MHz but can enhance it by factors of up to 5 at higher wavelengths, where $\alpha = 0.3$ produces higher fluxes at all redshifts.

For $\alpha = 0.7$ and 0.3, the most optimistic FPs predict that 1 hr, 10 hr and 100 hr pointings by SKA could detect the quasar at 500 MHz at $z \lesssim 10.5, 12,$ and 13, respectively. At 1.5 GHz, the same SKA times

Table 1. Planned sensitivities (nJy/beam) for SKA1 at 500 MHz, 1.5 GHz, 6.5 GHz, and 12.5 GHz for 1 hr, 10 hr, and 100 hr integration times (top three rows; see Table 3 of Braun et al. 2019) and ngVLA (bottom three rows; Plotkin & Reines 2018).

	500 MHz	1.5 GHz	6.5 GHz	12.5 GHz
1 hr	4400	2000	1300	1200
10 hr	1391	632	411	379
100 hr	440	200	130	120
1 hr	—	382	220	220
10 hr	—	121	70	70
100 hr	—	38	22	22

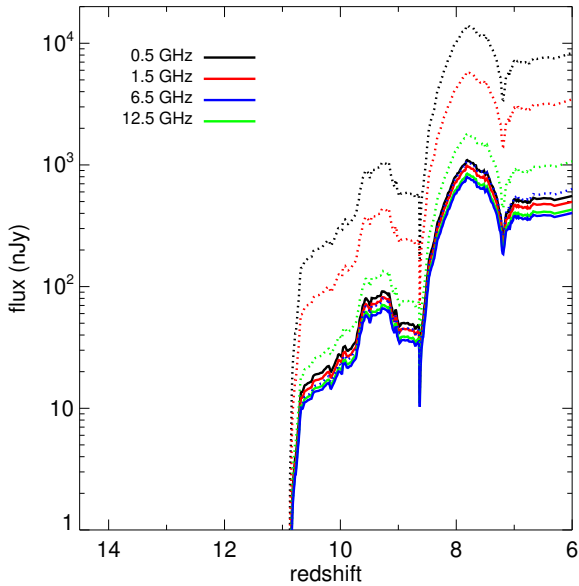


Figure 3. Left: radio emission at 0.5 - 12.5 GHz due to thermal bremsstrahlung from H II regions in star-forming regions in the host galaxy of the BH (solid lines). Right: non-thermal synchrotron emission from SNe (dotted lines).

could detect it at $z \lesssim 11$, 12, and 13 - 13.5 (hereafter, upper and lower limits in z are for $\alpha = 0.3$ and 0.7, respectively). The ngVLA could detect the quasar at $z \lesssim 12 - 13$, 13.5 - 14.2, and 15 - 15.5 if one extrapolates the plots to redshifts higher than those for which we had bolometric luminosities. At 6.5 GHz, SKA could detect the BH at $z \lesssim 10 - 11$, 11 - 12, and 12 - 14 with 1 hr, 10 hr and 100 hr integration times and ngVLA could detect it at 12 - 13, 13.5 - 14.2, and 14.2 - 15.5 if one again extrapolates the plots to higher z . At 12.5 GHz, SKA could detect the quasar at $z \lesssim 10 - 11$, 11 - 12, and 12 - 13.5 with 1 hr, 10 hr and 100 hr pointings and ngVLA could detect it at 11 - 12.8, 12.5 - 14, and 14 - 15.2. LOFAR could observe the quasar at $z \lesssim 10$ at 500 MHz.

We show H II region radio fluxes for the host galaxy in Figure 3. They are similar in strength because of their weak dependence on frequency. There is essentially no radio emission from the host galaxy until the onset of star formation at $z \sim 11$. It then rises from ~ 1 nJy at $z = 10.8$ to a first peak of $\sim 10^2$ Jy at $z = 9 - 10$ and then a second peak of ~ 103 Jy at $z = 8$. The peaks and dips in the radio flux in all four bands correspond to those in the SFRs in Figure 1. In reality, there is almost certainly some radio emission from the host galaxy at $z > 11$ because Smidt et al. (2018) could not resolve the formation of smaller star-forming regions at earlier times. However, as discussed in the previous section, this emission is expected to be at most a few nJy in the primordial gas. Radio emission due to thermal bremsstrahlung depends on electron temperatures and densities, so our fluxes should be taken as upper limits because H II regions in local galaxies, from which our estimates are taken, probably have higher densities than those in the host galaxy. The H II region flux at its two peaks is at most 10% of the flux from the SMBH.

The SN fluxes are 2 - 10 times higher than the H II region fluxes at the same frequencies at a given redshift. They exhibit the same dependence on SFR as the H II region emission. They somewhat exceed the two most pessimistic BH fluxes but the more optimistic BH fluxes can be 10 - 30 times higher in all four frequency bands. However, as discussed earlier, because we assume that all star formation results in SNe, these should be taken to be extreme upper limits.

The BH flux is likely to be much higher than the SN and H II region fluxes combined at $z \lesssim 11$. They could make the quasar easier to detect when present but not increase the redshifts at which it could be found.

4 DISCUSSION AND CONCLUSION

The first quasars are better candidates for radio followup after being detected at other wavelengths than being discovered in blind radio surveys because their areal densities on the sky are so small, $\sim 10^{-3}$ deg $^{-2}$ at $z > 7$ (Wang et al. 2021; Nanni et al. 2022). The SKA-MID and ultra deep surveys will reach sensitivities of 200 nJy and 50 nJy (Table 1 of Prandoni & Seymour 2014) so they could in principle detect quasars at $z \lesssim 14$, but it is unlikely that any would fall in the 10 - 30 deg 2 and 1 deg 2 patches of the sky they will cover. ngVLA radio surveys will reach sensitivities of 45 nJy at 3.5 - 12.3 GHz and 78 nJy at 1.2 - 3.5 GHz with 24 hr integration times, but with typical allocations of a few thousand hours a survey at this depth would cover $\lesssim 100$ deg 2 and probably not find BHs at high redshifts.

The properties of our quasar are similar to those of other $z > 7$ BHs (see Table 1 and Figure 8 of Fan et al. 2022), so our fluxes are likely typical of SMBHs of this era. Many quasars at $z > 6$ have larger masses so our estimates could be on the low side at these redshifts. Radio measurements by Momjian et al. (2014) impose 3σ upper limits of 23 μ Jy on the 1.4 GHz rest-frame flux of J1120, which is consistent with the lower end of the FPs such as BON13 and our H II region continuum fluxes, which are about 20 μ Jy. The higher end of our radio fluxes are on par with those recently reported for several $z \sim 6$ quasars. Bañados et al. (2021) measured flux densities of 0.31 - 2.9 mJy at 1.4 GHz for J2228+0110, J1427+3312, J1429+5447 and P172+18 at $z = 5.95 - 6.82$. Zhang et al. (2022) report a flux density of 5.5 mJy for the radio-loud AGN VIK J2318-3113 at $z = 6.44$. These fluxes are a factor of a few higher than those of the more optimistic FPs we considered but these sources are thought to be blazars that are unusually radio-loud. In particular, very-long baseline interferometry determined that the radio emission from J2318-3113 originated from a nuclear region about 1 pc across, indicating that the emission was due to the BH itself and not radio jets.

If the quasar has jets there could be additional radio flux due to synchrotron emission from its lobes that we do not consider here. However, except for one or two rare cases in which compact jets have been observed from high-redshift quasars on scales of a kpc or less (Momjian et al. 2018; Connor et al. 2021), jets are not expected for most of these sources. They have generally been observed at $L_{\text{bol}} \lesssim 0.01 L_{\text{Edd}}$ and $L_{\text{bol}} \gtrsim L_{\text{Edd}}$ and SMBHs must grow at rates of 0.1 - 1 \dot{M}_{Edd} to become quasars by $z \sim 6$. The BH in our model accretes at 0.2 L_{Edd} - 0.9 L_{Edd} over its lifetime. If a jet did form, the cosmic microwave background (CMB) would probably quench its emission (Ghisellini et al. 2014; Fabian et al. 2014) but not the FP fluxes because they originate from the central region of the quasar.

SKA and ngVLA will probe the properties of the first quasars at much earlier stages of evolution in the coming decade, discriminating between seeding mechanisms such as birth as DCBHs or prompt formation during galaxy mergers (e.g., Mayer et al. 2010). The ngVLA will be the better observatory for following up on quasar candidates previously discovered with other telescopes because it can detect them at up to $z \sim 16$ with 100 hr pointing times while SKA will be limited to $z \sim 14$. They will also complement NIR surveys by eliminating BH impostors, since strong radio emission would not be expected from active SF in early galaxies alone. SKA and the ngVLA

will, together with *JWST*, *Euclid* and the *RST*, will inaugurate the era of $z \sim 15$ quasar astronomy in the coming decade.

ACKNOWLEDGEMENTS

We thank the anonymous referee, whose critique improved the quality of this work. M. A. L. thanks the UAEU for funding via UPAR grant No. 31S390 and startup grant No 31S372. This work was also supported by the program Unidad de Excelencia María de Maeztu CEX2020-001058-M.

5 DATA AVAILABILITY STATEMENT

The data in this study will be made available upon request to the corresponding author.

REFERENCES

- Bañados E., et al., 2021, *ApJ*, 909, 80
 Bañados E., et al., 2023, *ApJS*, 265, 29
 Belladitta S., et al., 2020, *A&A*, 635, L7
 Bogdan A., et al., 2023, doi:10.48550/arXiv.2305.15458, p. arXiv:2305.15458
 Bonchi A., La Franca F., Melini G., Bongiorno A., Fiore F., 2013, *MNRAS*, 429, 1970
 Braun R., Bonaldi A., Bourke T., Keane E., Wagg J., 2019, doi:10.48550/arXiv.1912.12699, p. arXiv:1912.12699
 Condon J. J., 1992, *ARA&A*, 30, 575
 Condon J. J., Cotton W. D., Broderick J. J., 2002, *AJ*, 124, 675
 Connor T., et al., 2021, *ApJ*, 911, 120
 Fabian A. C., Walker S. A., Celotti A., Ghisellini G., Mocz P., Blundell K. M., McMahon R. G., 2014, *MNRAS*, 442, L81
 Fan X., Banados E., Simcoe R. A., 2022, doi:10.48550/arXiv.2212.06907, p. arXiv:2212.06907
 Ghisellini G., Celotti A., Tavecchio F., Haardt F., Sbarro T., 2014, *MNRAS*, 438, 2694
 Gloude-mans A. J., et al., 2021, *A&A*, 656, A137
 Gloude-mans A. J., et al., 2022, *A&A*, 668, A27
 Gültekin K., Cackett E. M., Miller J. M., Di Matteo T., Markoff S., Richstone D. O., 2009, *ApJ*, 706, 404
 Gültekin K., Cackett E. M., King A. L., Miller J. M., Pinkney J., 2014, *ApJ*, 788, L22
 Gültekin K., King A. L., Cackett E. M., Nyland K., Miller J. M., Di Matteo T., Markoff S., Rupen M. P., 2019, *ApJ*, 871, 80
 Herrington N. P., Whalen D. J., Woods T. E., 2023, *MNRAS*, 521, 463
 Hosokawa T., Yorke H. W., Inayoshi K., Omukai K., Yoshida N., 2013, *ApJ*, 778, 178
 Jørgensen C. C., Almgren A., Bell J., Heger A., Whalen D., Woosley S. E., 2010, *ApJ*, 709, 11
 Kennicutt Robert C. J., 1998, *ARA&A*, 36, 189
 Körding E., Falcke H., Corbel S., 2006, *A&A*, 456, 439
 Latif M. A., Whalen D. J., Khochfar S., Herrington N. P., Woods T. E., 2022a, *Nature*, 607, 48
 Latif M. A., Whalen D., Khochfar S., 2022b, *ApJ*, 925, 28
 Lupi A., Haiman Z., Volonteri M., 2021, *MNRAS*, 503, 5046
 Marconi A., Risaliti G., Gilli R., Hunt L. K., Maiolino R., Salvati M., 2004, *MNRAS*, 351, 169
 Mayer L., Kazantzidis S., Escala A., Callegari S., 2010, *Nature*, 466, 1082
 McGreer I. D., Becker R. H., Helfand D. J., White R. L., 2006, *ApJ*, 652, 157
 Meiksin A., Whalen D. J., 2013, *MNRAS*, 430, 2854
 Merloni A., Heinz S., di Matteo T., 2003, *MNRAS*, 345, 1057
 Mezcua M., Hlavacek-Larrondo J., Lucey J. R., Hogan M. T., Edge A. C., McNamara B. R., 2018, *MNRAS*, 474, 1342
 Momjian E., Carilli C. L., Walter F., Venemans B., 2014, *AJ*, 147, 6
 Momjian E., Carilli C. L., Bañados E., Walter F., Venemans B. P., 2018, *ApJ*, 861, 86
 Mortlock D. J., et al., 2011, *Nature*, 474, 616
 Nanni R., Hennawi J. F., Wang F., Yang J., Schindler J.-T., Fan X., 2022, *MNRAS*, 515, 3224
 Pacucci F., Ferrara A., Volonteri M., Dubus G., 2015, *MNRAS*, 454, 3771
 Planck Collaboration et al., 2016, *A&A*, 594, A13
 Plotkin R. M., Reines A. E., 2018, doi:10.48550/arXiv.1810.06814,
 Plotkin R. M., Markoff S., Kelly B. C., Körding E., Anderson S. F., 2012, *MNRAS*, 419, 267
 Prandoni I., Seymour N., 2014, doi:10.48550/arXiv.1412.6942,
 Smidt J., Whalen D. J., Johnson J. L., Surace M., Li H., 2018, *ApJ*, 865, 126
 Spingola C., Dallacasa D., Belladitta S., Caccianiga A., Giroletti M., Moretti A., Orienti M., 2020, *A&A*, 643, L12
 Tenneti A., Di Matteo T., Croft R., Garcia T., Feng Y., 2018, *MNRAS*, 474, 597
 Valentini M., Gallerani S., Ferrara A., 2021, *MNRAS*, 507, 1
 Vikaeus A., Whalen D. J., Zackrisson E., 2022, *ApJ*, 933, L8
 Wang F., et al., 2021, *ApJ*, 907, L1
 Whalen D. J., Fryer C. L., 2012, *ApJ*, 756, L19
 Whalen D., Abel T., Norman M. L., 2004, *ApJ*, 610, 14
 Whalen D., van Veelen B., O’Shea B. W., Norman M. L., 2008, *ApJ*, 682, 49
 Whalen D. J., Mezcua M., Meiksin A., Hartwig T., Latif M. A., 2020a, *ApJ*, 896, L45
 Whalen D. J., Surace M., Bernhardt C., Zackrisson E., Pacucci F., Ziegler B., Hirschmann M., 2020b, *ApJ*, 897, L16
 Whalen D. J., Mezcua M., Patrick S. J., Meiksin A., Latif M. A., 2021, *ApJ*, 922, L39
 Willott C. J., et al., 2010, *AJ*, 139, 906
 Woods T. E., Patrick S., Elford J. S., Whalen D. J., Heger A., 2021, *ApJ*, 915, 110
 Yang J., et al., 2020, *ApJ*, 897, L14
 Zhang Y., An T., Wang A., Frey S., Gurvits L. I., Gabányi K. É., Perger K., Paragi Z., 2022, *A&A*, 662, L2

This paper has been typeset from a \LaTeX file prepared by the author.